Numerical analysis of the inhomogeneous current transport properties of $Ag/Bi_2Sr_2Ca_2Cu_3O_{10}$ tapes

Kazuhiro Ogawa* and Kozo Osamura
Department of Materials Science and Engineering, Kyoto University, Sakyo, Kyoto 606-8501, Japan
(Received 24 December 2002; published 8 May 2003)

The numerical analysis based on the two-dimensional weak link network model is carried out to investigate the influence of the microscopic inhomogeneities on *I-V* characteristics of the Ag/Bi2223 tapes. The dependence of *I-V* curves on the various parameters of the model (system size, effective coordination number, volume fraction, and connectivity) is calculated and statistical matters are discussed. It is revealed that the lattices having larger coordination number *Z* show better properties and volume fraction of superconducting (SC) phase is very important to have finite (nonzero) I_c. This indicates that it is very effective for improving the properties of the tapes to fabricate the tapes consisting of large *Z* grains and having high volume fraction of SC phase.

DOI: 10.1103/PhysRevB.67.184509 PACS number(s): 74.81.−g, 74.72.Hs

I. INTRODUCTION

Superconducting Ag/Bi2223 tapes are eminently suitable for many power applications and electric devices and actually, they have appeared on the market in recent years. However, because of many difficulties in manufacturing process, it is hard to say that the products make the most of the potential of the superconductor. Their *I-V* characteristics are regarded as one of the performance indicating factors of the tapes. It has a feature that the electric field is moderately generated in the vicinity of its critical current (I_c), suggesting that the transition from superconducting (SC) state to nonsuperconducting (non-SC) state is not sharp. In a practical point of view, this transition is desired to be an abrupt one. Therefore it is important to elucidate the mechanisms leading the characteristics to such behavior. This feature is suggested to be affected by a complicated microscopic current transport over the tapes which is related to the local non-SC transition caused by the inhomogeneities in the tapes. In order to improve the property, it is important to clarify the microscopic current transport properties of the tapes in detail. In other words, we must find how the microscopic inhomogeneities affect and change the overall current transport.

Weak links at homophase grain boundaries are regarded as one of the factors limiting the transport properties of Ag/Bi2223 tapes. At those boundaries, the local current is limited by de-coupling of Cooper pair and flux flow. It is known that the weak links form various shapes of network in the tapes and the strength level of I_c at each weak link is widely distributed because of the inhomogeneities (for example, different orientation angles at tilt and twist grain boundaries) in the sample. Sivakov *et al.* reported the investigated results of the spatial distribution of critical current densities in the filaments of Ag/Bi2223 multifilamentary tapes using low-temperature scanning laser microscope.[1] In their report, they concluded that Josephson weak links are one of the current limiting factors of the tapes.

The current is thought to be fond of flowing through the route that makes the least loss. In such an inhomogeneous system, in what manner does the current flow? How do the number and location of the weak links determine the current flowing path and the generation of voltage over the sample? Thus it is very interesting to investigate how the weak links affect the generation of electric field or the *I-V* characteristics of the tapes. Indeed, many researchers have studied the behavior of the weak links in Ag/Bi2223 tapes. By theoretical approaches, many researchers studied the inhomogeneous current distribution of the Bi system so far. The brick-wall model,[2,3] the railway switch model,[4,5] and the freeway model[6] are some of the examples.

Many oxide superconductors have anisotropic current transport properties and supercurrents flow preferentially in the *ab* plane. Particularly in tape-shaped samples, crystal grains have *c* aligned, perpendicular to the tape surface microstructures and their homophase grain boundaries act as weak links. Taking these into account, it is suggested that the current transport in tape samples gives quasi-two-dimensional behavior with weak link network along the broad face of the tape. For example, in Ag/Bi2223 tapes, platelike grains with dimensions of $10\times10\times1$ μm^3 are included by 4×10^6 in the sample volume of $10\times4\times0.02$ mm^3, which we usually use with respect to *I-V* measurements. There exist so many grains in the tapes that a statistical treatment is highly requested. Making use of these, and owing to the recent great progress in computers, numerical analysis of *I-V* characteristics of oxide superconductors with presumptive space lattices are performed by many researchers. The representative of the lattices used in such reports are square,[7–13] hexagonal,[14–17] and simulated real lattice based on electron backscatter diffraction pattern map.[18,19] The examined matters in those reports are various—calculation of *I-V* characteristics, evaluation of I_c, scaling law, etc. However, there are few systematized reports exclusively focused on Bi system.

Therefore, in the present paper, the object of our analysis is fixed to Ag/Bi2223 tapes and numerical analysis is carried out on the basis of the two-dimensional model. In the model, we regard grain boundaries as weak links and tapes are regarded as SC and non-SC elements connected by weak links with coordination number *Z*. On the basis of the model, cur-

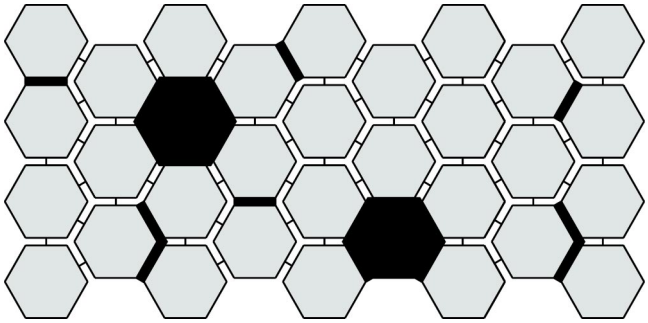

FIG. 1. Schematic figure of the weak link network. Symbols and straight lines represent SC or non-SC elements (gray: SC; black: non-SC) and weak links (thin: SC; bold: insulating), respectively. The current runs to the right.

rent transport in the tapes was calculated by accounting for probability distribution. Further the influence of the difference in the critical current distribution originating from local inhomogeneities at weak links upon the I-V characteristics over the sample, and current transfer properties in the tapes are investigated.

II. MODEL

A. System

In order to simplify the discussion, we treat a single grain as an element in the system of the model. Further we regard Ag/Bi2223 tapes as the systems consist of a large number of elements linked by weak links. The shape of the elements is, for the simplicity, assumed to be regular hexagon because it has the maximum angle among the regular polygon by which a plane can be laid all over. In the systems, M elements are in a column and N ones are in a row. The schematic figure of the systems is presented in Fig. 1.

This figure represents an overlooking view of the tapes. The current runs to the right and the reverse current flow is not taken into consideration. In the experimental samples, there are not only SC phases (Bi2223) but also voids, cavities[20] or non-SC phases like CuO. In order to take this into consideration, we introduce the probability whether each element is SC or not, namely the volume fraction V_f of Bi2223 phase. According to V_f, each element is divided into SC ones (gray symbols in the figure) and non-SC ones (black symbols in the figure). In addition, since there exist perfectly non-SC (insulating) links because of its bad alignment or residual carbon around there, we introduce the effective coordination number Z. It represents the averaged number of SC links come out from one element and $(6-Z)/6$ of the all links are suggested to be insulating links (bold lines in the figure). This is the system we use in numerical analysis.

B. Voltage

In this subsection, how the voltage generation is considered in the model is stated. When the transport current is applied to the sample, at the weak links where the current exceeds the I_c of the links, the transition from SC state to non-SC state occurs. In other words, since the I_c have a distribution, weak links are divided into SC ones and non-SC ones according to a certain probability when the current is applied. We express this probability of transition to non-SC state as p. After all links are divided into SC and non-SC ones according to p, whether the voltage is generated or not is determined as follows.

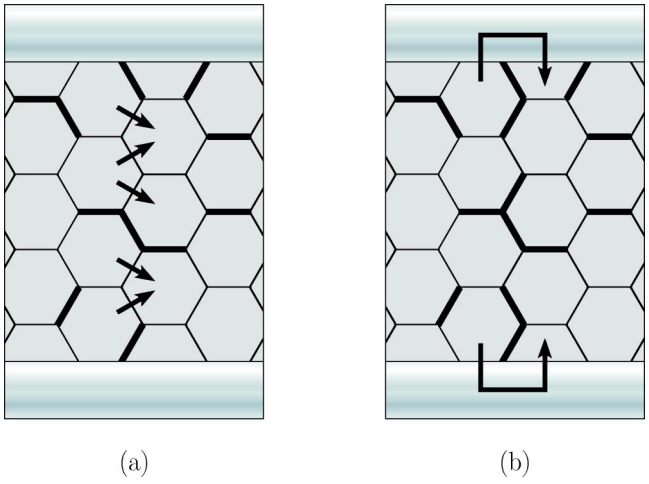

FIG. 2. The connectivity C and the voltage generation between a column and the next. This figure corresponds to the case $C=2$. Hexagonal symbols are SC elements. Bold lines are non-SC weak links or insulating ones. (a) Electric field is *not* generated. Arrows represent supercurrent paths. (b) Electric field is generated. Black arrows mean the current detour to Ag sheath.

As illustrated in Fig. 2, we focus on the column of weak links connecting elements along current flowing direction (more accurately, 30° inclined direction). As the applied current increases, the number of the links that state become non-SC increases. When fairly large number of weak links break, all links included in a column happen not to be supercurrent paths and the current cannot flow from one column to the next (from left to right) without dissipation. In short, an electric field is generated. In the calculation, we assume that the voltage generated in the system is caused by the Joule energy loss following the detour of current into Ag sheath that has less resistivity than normal state oxide. Here, we leave energy dissipations by flux flow out of consideration. Strictly speaking, the resistivity is regarded as the summation of the resistance of Ag sheath and the contact resistance at the interface with superconducting layer. However, because of the following reason, the contribution from the interface is ignored in this study. When it is supposed that the interface area (S_i) is 4×10^{-4} cm^2 (the width of the tape times the diameter of grains), the contact resistance ρ_i/S_i [contact resistivity $\rho_i=10^{-11}\ \Omega\cdot\mathrm{cm}^2$ (Ref. 21)] is estimated to be the same order with the resistance of the Ag sheath (described elsewhere in Sec. II E) and the exact value of S_i is very difficult to assess qualitatively.

In the actual current flow, when the current concentrates on narrow spaces, the current density at such position is locally increased and the transition from the SC to the non-SC state would occur. In order to take this into consideration, we introduce the connectivity C (which corresponds to the inverse of the current carrying capacity) and judge whether

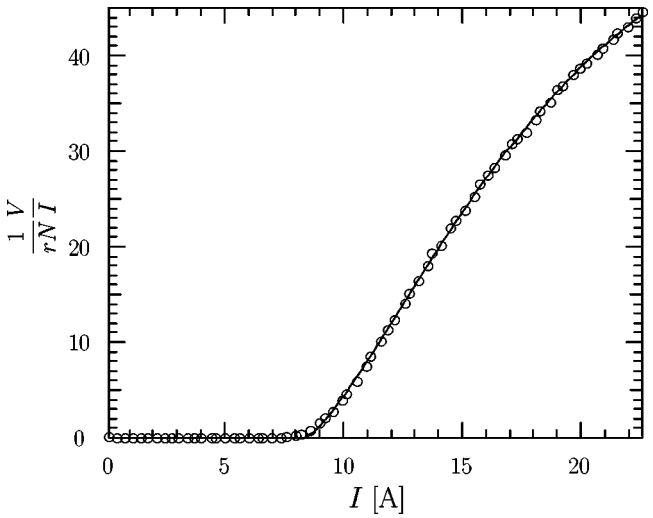

FIG. 3. Experimental curve and the fitted WDF. Circles are measured data and the thin line is once integrated WDF [Eq. (4)].

voltage is generated or not. For example, we explain the $C=2$ case. When more than two ($C=2$) SC weak links along transverse direction are connected like Fig. 2(a), the voltage is not generated. When such patterns do not exist, like Fig. 2(b), the current detour into Ag and the voltage is generated.

C. Calculation procedure

The calculation procedure is as follows:

(i) The number of elements M and N, effective coordination number Z, and connectivity C are voluntarily fixed and $(6-Z)/6$ of the all links are set to insulating links spatially at random.

(ii) Volume fraction V_f of SC elements is fixed. In accordance with V_f, SC elements and non-SC elements are spatially distributed at random.

(iii) The probability of being non-SC link, p, is determined (initially $p=0.0$ and increased as calculation proceeds) and in accordance with p, weak links are divided into SC ones, and non-SC ones spatially at random.

(iv) It is examined whether supercurrent penetrates from the ith weak link column perpendicular to the current direction to the next column or not according to the manner explained in the previous subsection. This is executed for $i=1$ to N and the proportion of voltage generating column W is calculated.

The procedure mentioned above is repeated as follows. (i)→(ii)→(*iii*)→(iv)→(add Δp to the probability p) →(iii)→(iv)→(add Δp to p) (iii)→(iv)→· · · . Finally, we obtain a p-W curve. The initial value of p is set to 0.0 and Δp is set to 0.001. The calculation is performed until p comes to 1.0. In the calculation, the process is assumed to be non-Markov one. Once a weak link becomes non-SC state, it never returns to be SC state until the calculation will be completed. In this report, this set of calculation is repeated 50 times and averaged data are converted into an I-V curve according to the method described in the next subsections.

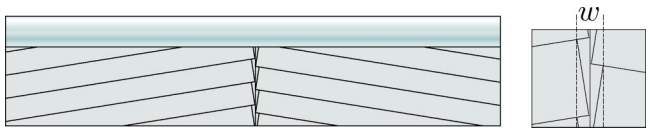

FIG. 4. Schematic figure of grain boundary. The grain boundary width w is illustrated. Effective barrier thickness d is defined as $d=w+2\lambda_{ab}$.

D. Conversion of p into I

In this and the next subsection, the way to convert the p-W curve into the I-V curve is proposed. In this subsection, p is converted to I and the next subsection, W is converted to V.

The transition probability p would be regarded as the function of transport current I, temperature T, and magnetic field B. In this report, T and B are assumed to be fixed and p could be expressed as $p=P(I)$. Since critical currents at weak links are distributed in accordance with some probability distribution function $f(I)$, $P(I)$ is expressed as

$$P(I)=\int_0^I f(I)dI. \tag{1}$$

Therefore, if we fix $f(I)$, we can convert p into I from the equation

$$I=P^{-1}(p). \tag{2}$$

Thus the p-W curve is converted into the I-W curve. This curve expresses the proportion of the columns which have no SC paths against the transport current.

Since the exact shape of the function $f(I)$ is uncertain now, we assume as $f(I)$ the Weibull distribution function (WDF),[22] which means the distribution of critical currents in a one-dimensional weak link chain. The expression of WDF is

$$g(I)=m\frac{L}{L_0|I_0|^m}(I-I_c^{\min})^{m-1}\exp\left[-\frac{L}{L_0|I_0|^m}(I-I_c^{\min})^m\right]. \tag{3}$$

Here, the parameters m, $I_c^{\min}$, and $L/L_0|I_0|^m$ denote shape factor, minimum critical current, and a constant, respectively. When the mechanism of the voltage generation is assumed to be the Joule energy loss,

$$\frac{n(I)}{N}=\int_{I_c^{\min}}^I g(I)dI=1-\exp\left[-\frac{L}{L_0|I_0|^m}(I-I_c^{\min})^m\right] \tag{4}$$

(N: number of weak links; $n(I)$: number of weak links in non-SC state when I is applied) is satisfied. Making use of this equation, the parameters are obtained from the experimental curve. Since

$$V=R(I)I=rn(I)I=rN\frac{n(I)}{N}I \tag{5}$$

is satisfied, from the equation

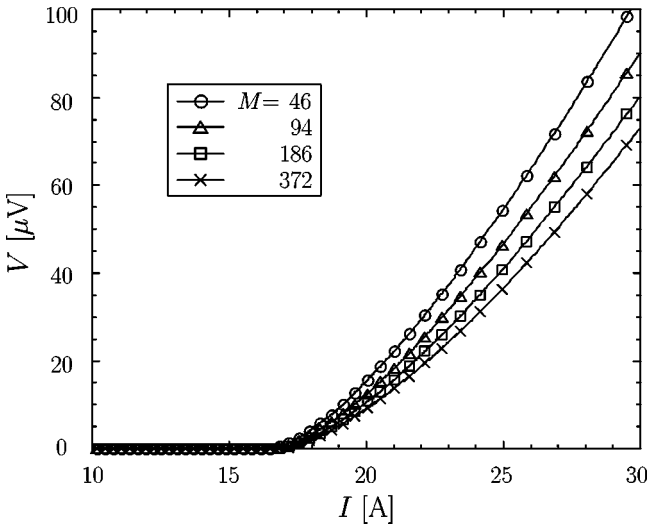

FIG. 5. Calculated results of *I-V* characteristics for the systems with different number of rows *M*.

$$\frac{n(I)}{N}=\frac{1}{rN}\frac{V}{I}=1-\exp\left[-\frac{L}{L_0|I_0|^m}(I-I_c^{\min})^m\right] \quad (6)$$

we can execute fitting by least-squares method. We made monocore Ag/Bi2223 tapes and took *I-V* measurements by the method described elsewhere in Ref. 23. As a result, we got the parameters $I_c^{\min}=8.34$ A, $m=1.37$, $L/L_0|I_0|^m=0.040$ for a sample measurement. In this paper, we use these parameters for the calculation. The experimental and fitted curve are displayed in Fig. 3. The other properties of the sample are as follows. I_c determined with the usual 1-μV/cm criterion is 7.62 A and the *n* value calculated by the slope of the log-log *I-V* curve between 0.1 and 1 μV is 20.4.

E. Conversion of *W* into *V*

In this subsection, the way to convert *W* into *V* is explained. When the current makes a detour into Ag sheath at the non-SC column, we calculate the voltage using the resistivity of Ag, ρ_{Ag} at each column. In this case, it is a question of to what extent the current flows spatially, or how long is the effective barrier width *d* of the grain boundaries. There is a report about current distribution between Ag and oxide in Ag/Bi2223 tapes using the one-dimensional two-layered model.[24] Cha *et al.* said that the ratio of the current flowing in Ag and oxide is very sensitive to the ratio of interfacial resistance and Ag resistance, and they referred to the relaxation distance just like an effective barrier width. However, in our report, the interfacial resistance is neglected and this is not applicable. We think therefore that *d* is expressed as the summation of the grain-boundary width *w* and the penetration depth of Bi2223 along the *ab* direction $\lambda_{ab}\approx 200$ nm.[25] The absolute value of *w* is estimated as follows. From the analysis using the x-ray pole figure, it is estimated that the averaged misorientation angle of Bi2223 grains along the *c* axis in our samples is nearly equal to 9°, so we propose the averaged structure depicted in Fig. 4. As defined in the figure, the grain boundary *w* has maximum value $w_{\max}=2t\sin\theta$, where *t* is the thickness of grains and θ is the misorientation angle. In this study, $\theta=9°$ and $t=1$ μm lead to $w_{\max}\approx 0.31$ μm, and the minimum value $w_{\min}=0$ μm. Hence we take an average and estimate $w=(w_{\max}+w_{\min})/2\approx 0.16$ μm. Taking this into account, we use the effective barrier thickness $d=w+2\lambda_{ab}$ and $d\approx 0.56$ μm. Thus the resistivity of each column is

$$r\equiv\rho_{Ag}\frac{d}{S_{Ag}}. \quad (7)$$

Here, $\rho_{Ag}=2.9\times10^{-7}$ Ω cm (at 77 K) (Ref. 26) and the cross section of Ag sheath perpendicular to the applied current $S_{Ag}=2.0\times10^{-3}$ cm^2 lead to $r=8.1\times10^{-9}$ Ω.

We define $n(I)$ as the number of columns which cannot pass through the supercurrent therefore $R(I)$ becomes

$$R(I)=rn(I)=rN\frac{n(I)}{N}=rNW. \quad (8)$$

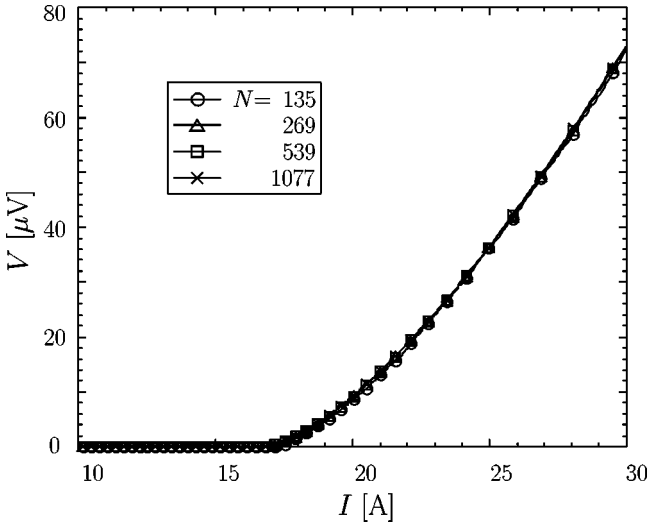

FIG. 6. Calculated results of *I-V* characteristics for the systems with different number of columns *N*.

TABLE I. I_c and *n* value dependence on *M*.

M	I_c (A)	*n*
46	17.1	64.4
94	17.3	74.0
186	17.4	76.2
372	17.5	69.1

TABLE II. I_c and *n* value dependence on *N*.

N	I_c (A)	*n*
135	17.7	97.2
269	17.6	77.5
539	17.6	73.0
1077	17.5	69.1

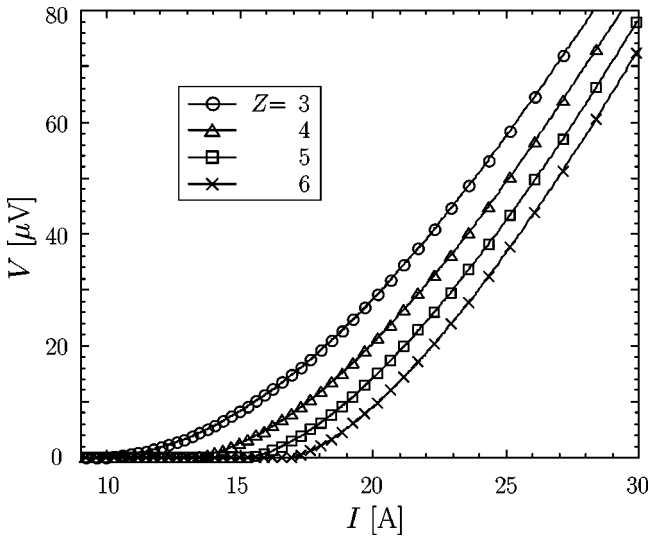

FIG. 7. Calculated results of *I*-*V* characteristics for the systems with different effective coordination number *Z*.

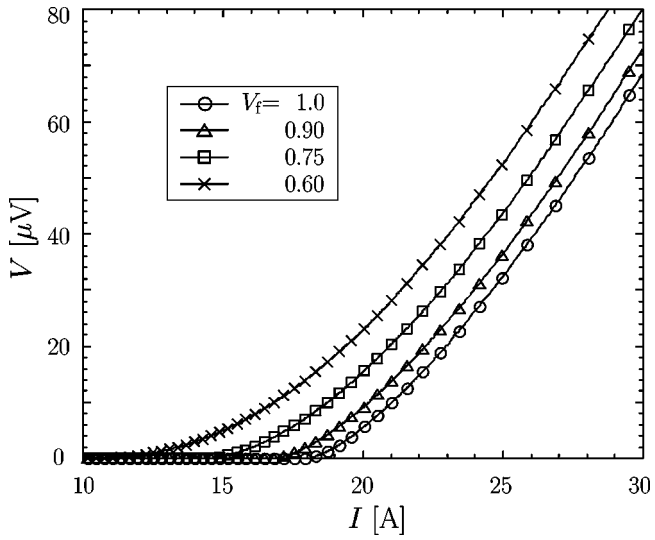

FIG. 8. Calculated results of *I*-*V* characteristics for the systems with different volume fractions V_f.

On the other hand, the generated voltage of the system is $V=R(I)I$. From those equations,

$$V=rNWI \tag{9}$$

is derived. By use of this Eq. (9), we convert *I*-*W* curve into *I*-*V* curve. From the converted curve, I_c is calculated using 1-μV/cm criterion and the *n* value is calculated by the slope of the log-log *I*-*V* curve between 0.1 and 1 μV.

F. Default parameters

In this subsection, we describe how to determine the default value of the five parameters *M*, *N*, *Z*, V_f, *C* before starting calculation. The broad surface of the sample used to be fabricated is about 10×4 mm^2 and platelike Bi2223 grains are about with dimension of 10×10 μm^2. Therefore we fix the element area which represents a single grain to 10×10 μm^2, resulting in the regular hexagon with one side $(200/3\sqrt{3})^{1/2}$ μm. The elements are laid all over the area 10×4 mm^2, and *M* and *N* are determined by executing a division. Namely, $M=372$ and $N=1077$ are used as the default parameters.

For the effective coordination number *Z* and the connectivity *C*, the ideal situation ($Z=6$ and $C=1$) is chosen for the default. For the volume fraction V_f, the average V_f of our samples, usually 0.90 is the default.

TABLE III. I_c and *n* value dependence on *Z*.

Z	I_c (A)	*n*
3	11.3	18.6
4	14.1	39.7
5	16.1	53.0
6	17.5	69.1

III. RESULTS AND DISCUSSION

In the following subsections, the calculated results of *I*-*V* curves and the effects of the change in each parameter are summarized.

A. System size *M* and *N*

In Figs. 5 and 6, the calculated dependence of *I*-*V* curves on the number of the rows *M* and on the number of the columns *N* are indicated. Moreover, I_c and the *n* value of each curve are listed in Tables I and II in detail.

In Fig. 6, the curves are normalized to $N=1077$ for comparison because they must be compared in the same voltage tap separation.

When the current increases, the electric field is moderately generated in the vicinity of its I_c for all curves. This behavior is qualitatively coincident with the experimental one. As seen in Fig. 5, it is revealed that the slope of the curves become more gradual (but the *n* value is not monotone decreasing) and I_c become higher in accordance with increasing *M*. It is the consequence of the fact that large *M* systems have many SC paths compared to the small *M* ones in the same column if the transition probability at each weak links is the same.

On the other hand, as shown in Fig. 6, the curves are similar for different *N*, apparently. However looking at the result Table II carefully, it can be found that I_c and the *n* values decrease in accordance with the increase in *N*. This tendency of the decrease in I_c is originated from the equivalence of the decrease in *N* and the relative increase in *M*. However, the opposite tendency in *n* values is inconsistent with what is expected by the relative increase in *M*. The reason might be that the absolute value of the generated voltage becomes larger with decreasing *N* when a column becomes non-SC and this effect is stronger than that caused by the relative increase in *M*.

TABLE IV. I_c and n value dependence on V_f.

V_f	I_c (A)	n
0.60	12.5	21.0
0.75	15.5	45.2
0.90	17.5	69.1
1.0	18.6	86.6

B. Effective coordination number *Z*

The calculated *I-V* characteristics for the systems with different coordination number *Z* are shown in Fig. 7. I_c and n values of each curves are listed in Table III in detail. As shown in the figure, larger *Z* system have steeper slope in the *I-V* curve and higher I_c. This is because the amount of the total current flowing without dissipation becomes larger when there are a lot of SC paths in the system. When fixed possibility p is given, it can be expected that the large *Z* elements have more SC paths than small *Z* ones have. Here, it would be noted that the important factor is not the total number of the links but the number of paths rooted from one grain. For example, the systems with ($Z=6, M=186, N=1077$), ($Z=6, M=372, N=539$), and ($Z=3, M=372, N=1077$) have almost the same number of the total links, but the characterisitics of the former two systems are extremely different from that of the latter one.

From the results, one would notice that both I_c and the n value are more sensitive to the parameter *Z* than to the parameter *M* or *N*. This indicates that it is important to make well-aligned grains, less carbon-resided and less precipitated grain boundaries for the improvement of the performance of the tapes.

C. Volume fraction V_f

The calculated *I-V* curves for the systems with four different volume fractions V_f is shown in Fig. 8 and detailed values of I_c and n values are in Table IV. The higher I_c and the larger n values are obtained for the higher V_f and this dependency is the same as the *Z* dependence. The increase of V_f is suggested to have the same effect as that of *Z* on *I-V* characteristics in the point of having many paths rooted from each grains. V_f has a strong effect on I_c and n values in comparison with *M* or *N* do as well as *Z*. It is revealed that the increase of the volume fraction makes a great contribution to the improvement of the sample.

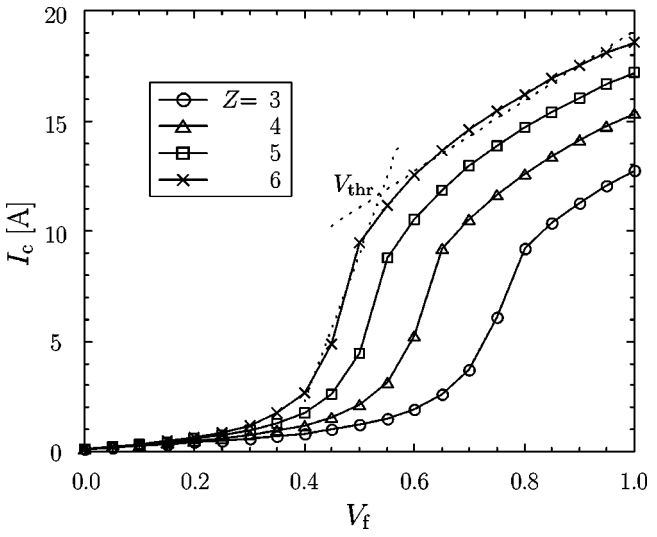

FIG. 9. Change of I_c as a function of volume fraction V_f for the systems with different effective coordination number *Z*. V_{thr} is the threshold of the volume fraction.

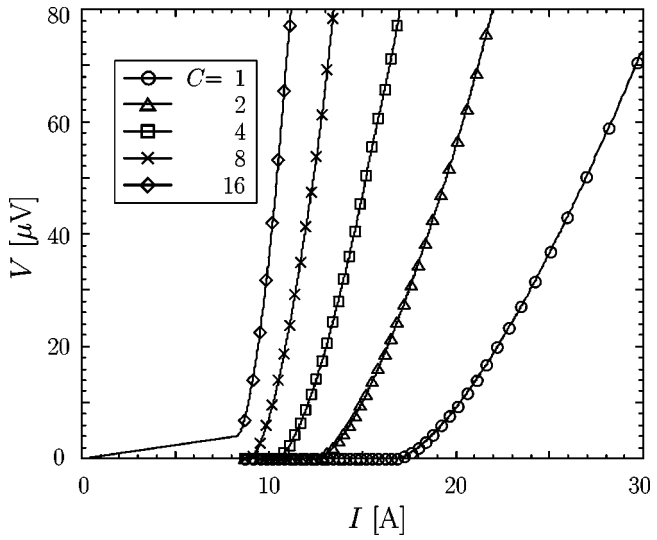

FIG. 10. Calculated results of *I-V* characteristics for the systems with different connectivity *C*.

In order to investigate the effect of the change in V_f on the characteristics from a different point of view, the dependence of I_c on V_f is investigated. The results are shown in Fig. 9. As is shown in the figure, it is revealed that I_c drops in the vicinity of a certain threshold V_{thr} when V_f decreases. At $V_f=1.0$, all systems have $I_c>10$ A, but I_c drops in the vicinity of $V_{thr}=0.81$, 0.68, 0.59, 0.54 for $Z=3$, 4, 5, 6 system, respectively. It is revealed that the larger *Z* lattices need a smaller volume fraction of Bi2223 to have finite (nonzero) I_c than small *Z* ones need.

D. Connectivity *C*

In Fig. 10, the calculated dependence of *I-V* curves on the connectivity *C* is indicated. The detailed I_c and n value of each curve are listed in Table V. As *C* increases, I_c decreases abruptly and the n value is nearly the same for each system. *C* means the inverse of the current carrying capacity of each

TABLE V. I_c and n value dependence on *C*.

C	I_c (A)	n
1	17.5	69.1
2	13.1	72.0
4	10.8	85.3
8	9.3	81.7
16	2.0	

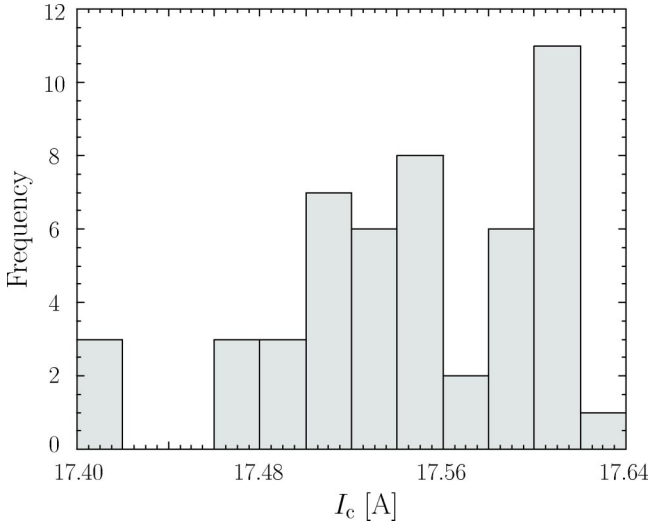

FIG. 11. Histogram of calculated I_c for 50 times independent trials.

element and this tendency indicates that I_c decreases in accordance with the decay of the ability to endure the current concentration.

E. Statistical matters

In numerical analysis with stochastic processes like the calculation in this report, the obtained results are dispersed, or different in each trial. In order to evaluate the degree of dispersion, we investigate the calculated I_c and n values with default parameters for 50 times independent trial. Results are shown in Figs. 11 and 12 in histogram. As shown in the figures, I_c and n values are scattered around the maximum likelihood value. The coefficient of variation which is the standard deviation divided by the average is 0.0031 for I_c and 0.18 for the n value. It is found that I_c have much less relative deviation than the n value. This tendency would be

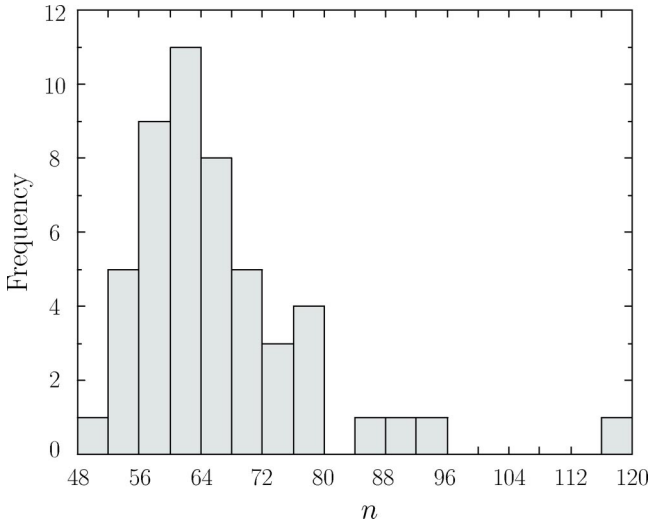

FIG. 12. Histogram of the calculated n value for 50 times independent trials.

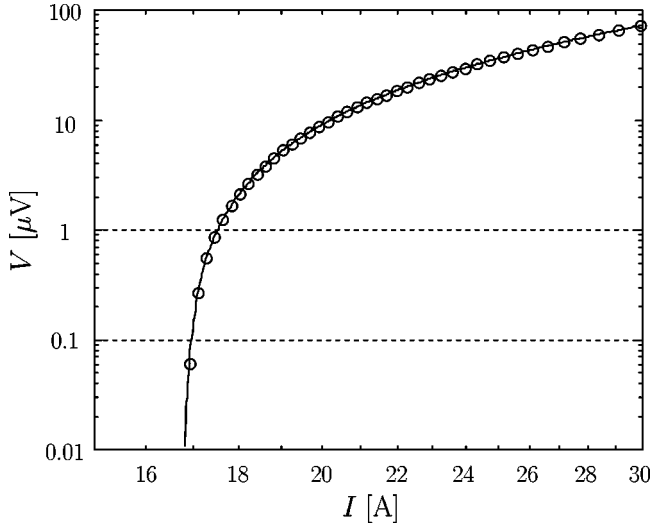

FIG. 13. Calculated I-V curve with default parameters in logarithmic coordinates.

related to the well-known results that n values have the large variability in experimental measurements.

The absolute magnitudes of n values obtained from the calculations seem to be generally larger than those obtained by the experiments. In order to discuss this phenomenon, the log-log plot of the calculated I-V curve with the default parameters is shown in Fig. 13. As appeared in the slope of the curve, the n value is largely affected by the range of voltage where the n value is calculated. In the figure, the voltage range used in the calculation is indicated by the dotted lines. In order to show that plainly, the first-order differential curve is indicated in Fig. 14. In this figure, the current range is indicated by the dotted lines. The n value is nearly equal to the average of the ordinates included in the range. Therefore if the range shifts to the right (to higher current or higher voltage), the n value becomes small, and vice versa. The result that the calculated values are larger than the experimental ones suggests the next possibilities: (i) The voltage value generated when a column becomes to non-SC is

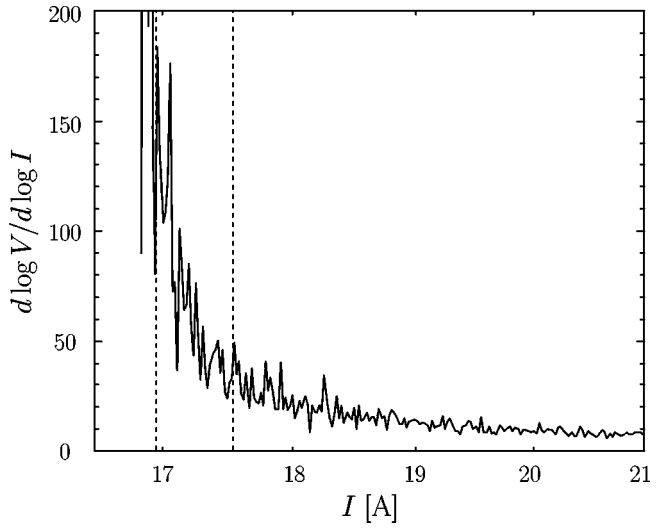

FIG. 14. First-order differential curve of log I-log V.

smaller, or, the effective barrier thickness d is thinner in reality than in the assumption we made. (ii) The real probability distribution function $f(I)$ has a wider shape than the assumed function.

IV. SUMMARY

In order to investigate the influence of the microscopic inhomogeneities like widely distributed I_c on I-V characteristics of the Ag/Bi2223 tapes, we have proposed a two-dimensional weak link network model and carried out numerical analysis. The following results are obtained: (i) It is revealed that the lattices having larger coordination number Z show better properties. (ii) Volume fraction is very important to have finite (nonzero) I_c. (iii) It is very effective for improving the properties to fabricate the tapes consisting of large Z grains and having high V_f of the SC phase.

ACKNOWLEDGMENT

This study was partially supported by the Japan Society for the Promotion of Science.

*Email address: robo@hightc.mtl.kyoto-u.ac.jp

[1] A.G. Sivakov, A.V. Lukashenko, D. Abraimov, P. Müller, A.V. Ustinov, and M. Leghissa, Appl. Phys. Lett. **76**, 2597 (2000).
[2] L.N. Bulaevskii, J.R. Clem, L.I. Glazman, and A.P. Malozemoff, Phys. Rev. B **45**, 2545 (1992).
[3] L.N. Bulaevskii, L.L. Daemen, M.P. Maley, and J.Y. Coulter, Phys. Rev. B **48**, 13 798 (1993).
[4] B. Hensel, J.-C. Grivel, A. Jeremie, A. Perin, A. Pollini, and R. Flukiger, Physica C **205**, 329 (1993).
[5] Y.H. Li, J.A. Kilner, M. Dhalle, A.D. Caplin, G. Grasso, and R. Flukiger, Supercond. Sci. Technol. **8**, 764 (1995).
[6] G.N. Riley, Jr., A.P. Malozemoff, Q. Li, S. Fleshler, and T.G. Holesinger, JOM **49**, 24 (1997).
[7] G. Blatter, J. Rhyner, and H. Dersch, Physica C **162-164**, 355 (1989).
[8] J. Rhyner and G. Blatter, Phys. Rev. B **40**, 829 (1989).
[9] R.A. Hyman, M. Wallin, M.P.A. Fisher, S.M. Girvin, and A.P. Young, Phys. Rev. B **51**, 15 304 (1995).
[10] M. Ziese, Phys. Rev. B **55**, 8106 (1997).
[11] R. Haslinger and R. Joynt, Phys. Rev. B **61**, 4206 (2000).
[12] H.A. Knudsen and A. Hansen, Phys. Rev. B **61**, 11 336 (2000).
[13] K. Osamura, K. Ogawa, T. Thamizhavel, and A. Sakai, Physica C **335**, 65 (2000).
[14] N.A. Rutter, B.A. Glowacki, and J.E. Evetts, Supercond. Sci. Technol. **13**, L25 (2000).
[15] E.D. Specht, A. Goyal, and D.M. Kroeger, Supercond. Sci. Technol. **13**, 592 (2000).
[16] N.A. Rutter and B.A. Glowacki, IEEE Trans. Appl. Supercond. **11**, 2730 (2001).
[17] B. Zeimetz, N.A. Rutter, B.A. Glowacki, and J.E. Evetts, Supercond. Sci. Technol. **14**, 672 (2001).
[18] J.E. Evetts, M.J. Hogg, B.A. Glowacki, N.A. Rutter, and V.N. Tsaneva, Supercond. Sci. Technol. **12**, 1050 (1999).
[19] B. Holzapfel, L. Fernandez, F. Schindler, B. Boer, N. Reger, J. Eickemeyer, P. Berberich, and W. Prusseit, IEEE Trans. Appl. Supercond. **11**, 3872 (2001).
[20] J. Jiang, X.Y. Cai, J.G. Chandler, M.O. Rikel, E.E. Hellstrom, R.D. Parrella, D. Yu, Q. Li, M.W. Rupich, J.G.N. Riley, Jr., and D.C. Larbalestier, IEEE Trans. Appl. Supercond. **11**, 3561 (2001).
[21] Y. Fang, S. Danyluk, M.T. Lanagan, C.A. Youngdahl, X. Xu, and K. Numata, Physica C **252**, 389 (1995).
[22] F. Irie, Y. Tsujioka, and T. Chiba, Supercond. Sci. Technol. **5**, S379 (1992).
[23] K. Osamura, H. Ito, T. Horita, S. Nonaka, H.D. Ramsbottom, and H. Okuda, Adv. Cryog. Eng. **44**, 427 (1998).
[24] Y.S. Cha, M.T. Lanagan, K.E. Gray, V.Z. Jankus, and Y. Fang, Appl. Supercond. **2**, 47 (1994).
[25] J.G. Ossandon, J.R. Thompson, Y.C. Kim, Y.R. Sun, D.K. Christen, and B.C. Chakoumakos, Phys. Rev. B **51**, 8551 (1995).
[26] Y. Fang, S. Danyluk, and M.T. Lanagan, Cryogenics **36**, 957 (1996).